Available online at www.sciencedirect.com

ScienceDirect

Nuclear and Particle Physics Proceedings 279–281 (2016) 79–86

www.elsevier.com/locate/nppp

Results of the ARGO-YBJ experiment in detection of gamma rays

Tristano Di Girolamo on behalf of the ARGO-YBJ collaboration

Università di Napoli "Federico II" and INFN - Sezione di Napoli, Complesso Universitario Monte S. Angelo, Via Cintia, 80126 Napoli, Italy

Abstract

The ARGO-YBJ air shower detector has been in stable data taking for five years at the YangBaJing Cosmic Ray Observatory (Tibet, P.R. China, 4300 m a.s.l.) with a duty cycle > 86% and an energy threshold of a few hundreds of GeV. Besides working in shower mode, the detector used the scaler mode technique, which can reach the minimum threshold of 1 GeV. In this paper a selection of results in gamma ray astronomy will be presented, including those from the study of the diffuse emission from the Galactic plane.

Keywords: air shower detectors, ARGO-YBJ experiment, gamma ray sources

1. The detector

The ARGO-YBJ experiment is located at Yangbajing (Tibet, P.R. China, 4300 m a.s.l.) and consists of a single layer of Resistive Plate Counters (RPCs) on a total area of about 110×100 m^2. The detector has a modular structure, the basic module being a cluster (5.7×7.6 m^2), made of 12 RPCs. Each RPC is read by 80 strips (6.75×61.8 cm^2) which are the space pixels, logically organized in 10 independent pads (55.6×61.8 cm^2) which are individually acquired and represent the time pixels of the detector [1]. The detector carpet is connected to two different data acquisition (DAQ) systems, which work independently: in shower mode, for each event the location and timing of each detected particle is recorded, allowing the reconstruction of the lateral distribution and of the arrival direction; in scaler mode, the counting rate of each cluster is measured every 0.5 s, with little information on the space distribution and arrival direction of the detected particles. The trigger of the shower mode was $N_{pad} \geq 20$ in a time window of 420 ns, with a rate of 3.5 kHz. In the scaler mode DAQ, for each cluster four scalers record the rate of counts ≥ 1, ≥ 2, ≥ 3 and ≥ 4 in a time window of 150 ns. The corresponding measured rates are, respectively, ~40 kHz, ~2 kHz, ~300 Hz and ~120 Hz [2]. The experiment has been taking data with its full layout from November 2007 to February 2013.

The detector pointing accuracy, angular resolution and absolute energy calibration have been determined studying the deficit in the cosmic ray flux due to the Moon. In particular, the opening angle ψ_{70}, containing 71.5% of the cosmic ray events from a point source, is about 2° for $N_{pad} \geq 20$, 1.36° for $N_{pad} \geq 60$ and 1.0° for $N_{pad} \geq 100$, while an improvement of $\sim 30-40\%$ is expected for gamma-induced showers because of their better defined time profile [3].

2. Sky survey

The ARGO-YBJ detector surveyed the northern hemisphere, in the declination band from -10° to 70°, at energies above 0.3 TeV. With an integrated sensitivity down to 0.24 Crab unit[1] (depending on the declination) after five years of data taking, six sources were detected with a statistical significance S>5 standard deviations (s.d.), and five excesses are reported as potential (S>4 s.d.) gamma ray emitters [4]. The list of excess regions, with their corresponding significances for $N_{pad} \geq 20$ (except ARGO J1841-0332, spatially consistent with the HAWC candidate 1HWC J1844-031c [5],

[1]The Crab unit here is defined as the integral flux 3.30×10^{-11} photons cm^{-2} s^{-1} above ~0.7 TeV

http://dx.doi.org/10.1016/j.nuclphysbps.2016.10.012

ARGO-YBJ Name	S (s.d.)	TeV Association
ARGO J0409-0627	4.8	
ARGO J0535+2203	20.8	Crab Nebula
ARGO J1105+3821	14.1	Mrk 421
ARGO J1654+3945	9.4	Mrk 501
ARGO J1839-0627	6.0	HESS J1841-055
ARGO J1907+0627	5.3	HESS J1908+063
ARGO J1910+0720	4.3	
ARGO J1912+1026	4.2	HESS J1912+101
ARGO J2021+4038	4.3	VER J2019+407
ARGO J2031+4157	6.1	MGRO J2031+41
		TeV J2032+4130
ARGO J1841-0332	4.2	HESS J1843-033

Table 1: List of ARGO-YBJ excess regions with corresponding statistical significances S and TeV associations. All significances are given for $N_{pad} \geq 20$ except that of ARGO J1841-0332, which is for $N_{pad} \geq 100$.

for which $N_{pad} \geq 100$) estimated with equation (9) of [6] and corresponding TeV associations, is given in Table 1.

In the following, a selection of results concerning the sources detected in the sky survey will be presented.

2.1. Crab Nebula

The differential energy spectrum obtained for this source in the range 0.3-20 TeV can be described by the power law $dN/dE = (5.2 \pm 0.2) \times 10^{-12}(E/2\ TeV)^{(-2.63\pm0.05)}$ photons cm^{-2} s^{-1} TeV^{-1}, which gives an integral flux above 1 TeV of 1.97×10^{-11} photons cm^{-2} s^{-1}. Figure 1 shows this spectrum compared with results from other experiments [7].

The light curve over five years, with a binning of 200 days, is compatible with a steady emission with a probability of 0.07. A correlation analysis with data collected in 4.5 years of observations in common with Fermi/LAT and divided in bins of 200 days gives a Pearson correlation coefficient $r = 0.56 \pm 0.22$. Figure 2 shows the percentage variation of the ARGO-YBJ flux with respect to the average value as a function of the corresponding variation of the Fermi/LAT flux, for the nine bins of the light curve.

The same analysis was carried out with different bin widths, ranging from 10 to 450 days, and the corresponding correlation coefficients increase from $r = 0.10 \pm 0.06$ (10 days) to $r = 0.59 \pm 0.23$ (450 days).

2.2. Mrk 501

During its five years of operation, ARGO-YBJ monitored Mrk 501 at energies above 0.3 TeV [8]. The largest flare was observed from October 2011 to April

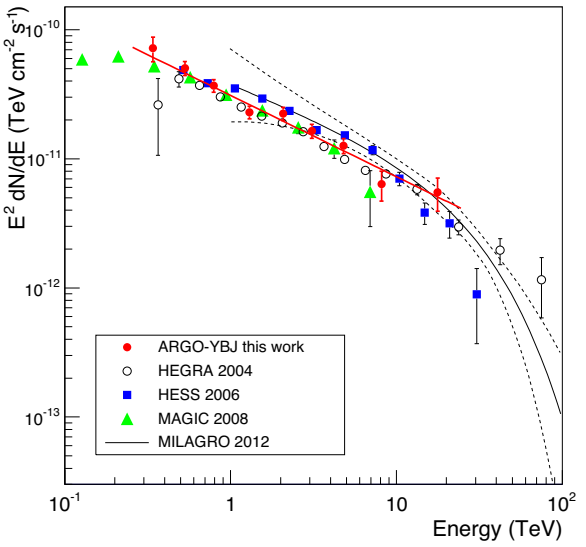

Figure 1: Crab Nebula differential energy spectrum multiplied by E^2 as measured by ARGO-YBJ and other experiments. The straight solid line represents the best fit of the ARGO-YBJ data, while the dotted lines delimitate the 1σ error band of the Milagro spectrum.

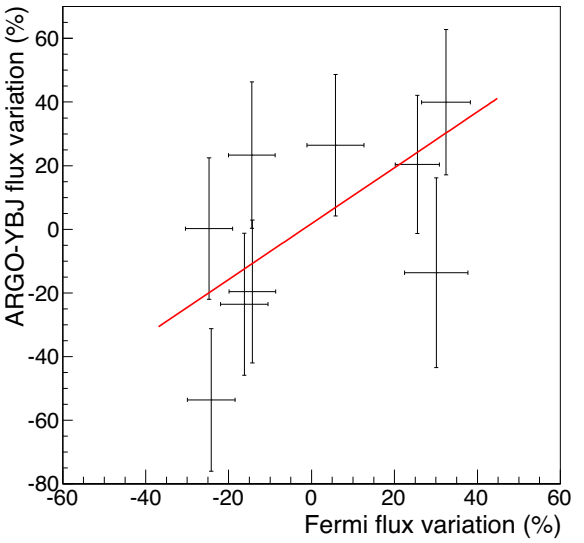

Figure 2: Percentage variation of the Crab Nebula flux with respect to the average value for ARGO-YBJ and Fermi/LAT data. The straight line represents the best fit $\Delta F_{ARGO} = (0.88 \pm 0.37)\Delta F_{Fermi} + (0.018 \pm 0.079)$.

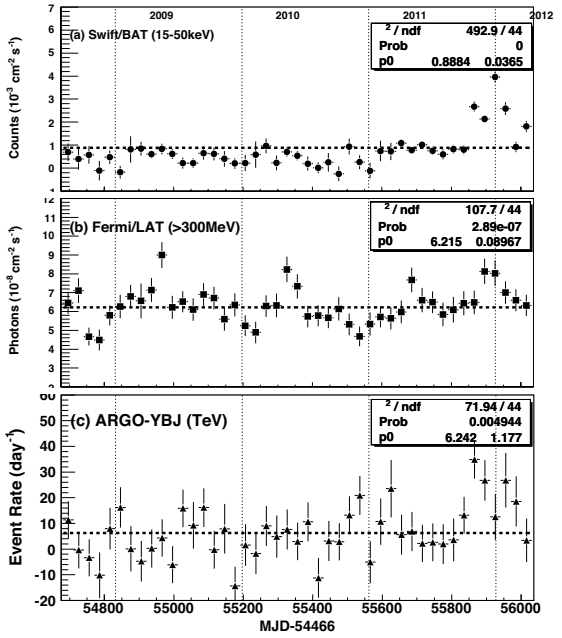

Figure 3: Light curves of Mrk 501 as measured by Swift/BAT, Fermi/LAT and ARGO-YBJ. Each bin contains 30 days, the vertical bars represent 1σ uncertainties, the horizontal dashed lines show the constant values resulting from fits.

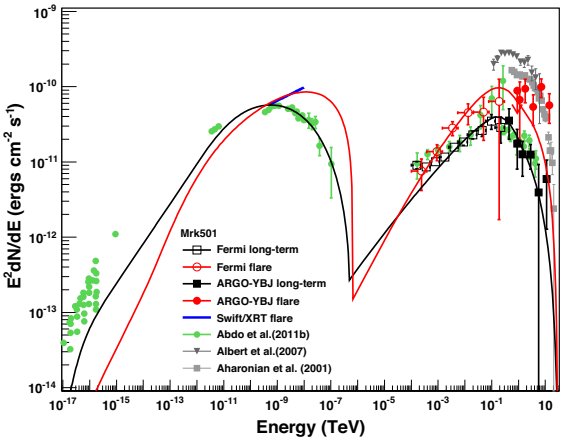

Figure 4: Spectral energy distribution of Mrk 501. The solid lines show the best fits to the data with a one-zone SSC model, the black curve corresponding to a model for the long-term averaged data, while the red curve describes the flaring data.

2012, with the brightest episode from October 17 to November 22, when the excess of the event rate reached 6.1 s.d., corresponding to ∼2 Crab units above 1 TeV, which means an increase to a flux 6.6±2.2 larger than the long-term steady one. The measured light curve, compared with those observed by Swift/BAT in the 15-150 keV range and by Fermi/LAT above 0.3 GeV, is given in Figure 3. During the X-ray flare at the end of 2011 (Swift/BAT flux enhanced by a factor ∼4) it is evident the increase of the TeV flux, while the GeV flux does not rise significantly.

ARGO-YBJ detected emission above 8 TeV with a significance larger than 4σ, which did not happen since the Mrk 501 flare in 1997 [9]. Considering the spectral energy distribution, which is given in Figure 4, a simple one-zone Synchrotron Self-Compton (SSC) model fits well the long-term data, however is unable to reproduce the flaring emission at energies >6 TeV due to the hardness of the spectrum.

A monitoring and study of flaring emission was carried out by ARGO-YBJ also for Mrk 421 [10].

2.3. Extended sources: the Cygnus region

The Cygnus region is the brightest portion of the gamma ray northern sky, where several complex structures have been observed at different wavelengths. This region is rich in potential cosmic ray acceleration sites, including Wolf-Rayet stars, OB associations, supernova remnants, pulsars, microquasars and superbubbles. Various Very High Energy (VHE) gamma ray sources have been detected within the Cygnus region, the brightest ones being the extended MGRO J2031+41/TeV J2032+4130 and MGRO J2019+37 [11], whose locations are consistent with two Fermi pulsars [12].

The significance map of the Cygnus region as observed by ARGO-YBJ using events with $N_{pad} > 20$ is shown in Figure 5 [13]. The four known TeV sources and the 24 GeV sources in the second Fermi/LAT catalogue are also marked in the figure. An excess is observed over a large part of the region, indicating a possible diffuse gamma ray emission (see next section).

A signal with a significance larger than 6 s.d. is detected at the position of MGRO J2031+41. The source extension is determined to be $\sigma_{ext} = (0.2^{+0.4}_{-0.2})^\circ$, consistent with the previous estimations by HEGRA [14] and MAGIC [15] experiments, i.e., $\sigma_{ext} = 0.103^\circ \pm 0.025^\circ$ and $\sigma_{ext} = 0.083^\circ \pm 0.030^\circ$, respectively. Assuming an intrinsic extension $\sigma_{ext} = 0.1^\circ$, the energy spectrum measured in the range 0.6-7 TeV is $dN/dE = (1.40 \pm 0.34) \times 10^{-11} (E/1\ TeV)^{(-2.83 \pm 0.37)}$ photons cm^{-2} s^{-1} TeV^{-1} and is reported in Figure 6. The integral flux above 1 TeV is ∼0.3 Crab unit, in agreement with Milagro results [16, 17] but about a factor 10 higher than the fluxes determined by HEGRA and MAGIC.

In a location consistent with MGRO J2031+41, Fermi/LAT detected a complex extended source, at-

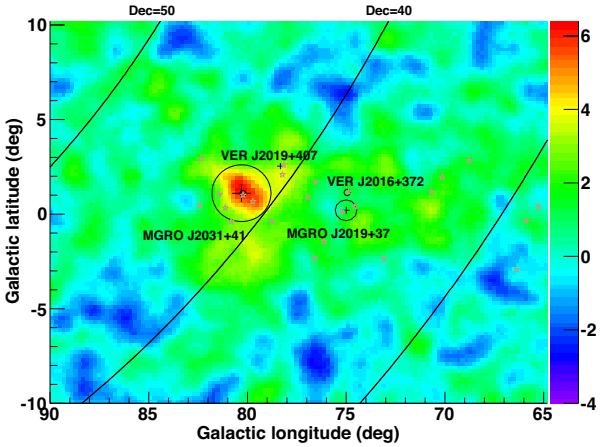

Figure 5: Significance map of the Cygnus region as observed by ARGO-YBJ. The four known VHE sources are reported. The errors on the MGRO source positions are given with crosses, while the circles indicate their intrinsic sizes. The open stars mark the location of the 24 GeV sources in the second Fermi/LAT catalogue.

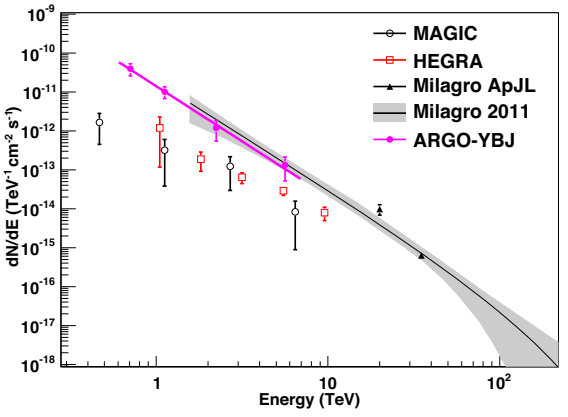

Figure 6: Spectrum of MGRO J2031+41 as measured by ARGO-YBJ and other experiments.

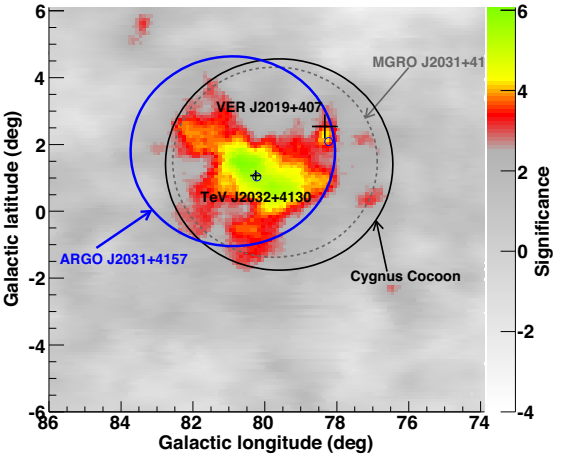

Figure 7: Significance map around ARGO J2031+4157 as observed by ARGO-YBJ. The large circles indicate the positions and 68% contours of ARGO J2031+4157, MGRO J2031+41 and the Cygnus Cocoon. The positions and extensions of TeV J2032+4130 [14] and VER J2019+407 [20] are marked with crosses.

tributed to the emission by a "cocoon" of freshly accelerated cosmic rays which fill the cavities carved by stellar winds and ionization fronts from young stellar clusters [18]. After reanalysing the complete ARGO-YBJ data set, subtracting the contribution of the overlapping TeV sources and using a larger region to evaluate the excess map (since Fermi/LAT observations revealed a large extended source), ARGO J2031+4157 resulted with an extension $\sigma_{ext} = 1.8^\circ \pm 0.5^\circ$, consistent with that of the Cygnus Cocoon as measured by Fermi/LAT, i.e., $\sigma_{ext} = 2.0^\circ \pm 0.2^\circ$ [19]. The ARGO-YBJ view of the Cygnus Cocoon region (for $N_{pad} \geq 20$) is given in Figure 7, where the largest statistical significance is 6.1 s.d., at the position of ARGO J2031+4157.

The spectrum also shows a good connection with that determined by Fermi/LAT in the 1-100 GeV energy range, as shown in Figure 8. Therefore, ARGO J2031+4157 is identified as the counterpart of the Cygnus Cocoon at TeV energies. The combined differential spectrum of Fermi/LAT and ARGO-YBJ data is fitted with the power law function $dN/dE = (3.5 \pm 0.3) \times 10^{-9} (E/0.1\ \ TeV)^{(-2.16 \pm 0.04)}$ photons cm^{-2} s^{-1} TeV^{-1} (dot-dashed line in Figure 8).

In order to reproduce the gamma ray emission from the Cygnus Cocoon, a purely hadronic model [21] can be adopted, in which the observed gamma rays are due to the decay of π^0 mesons resulting from inelastic collisions between accelerated protons and target gas. Assuming that the primary proton spectrum follows a

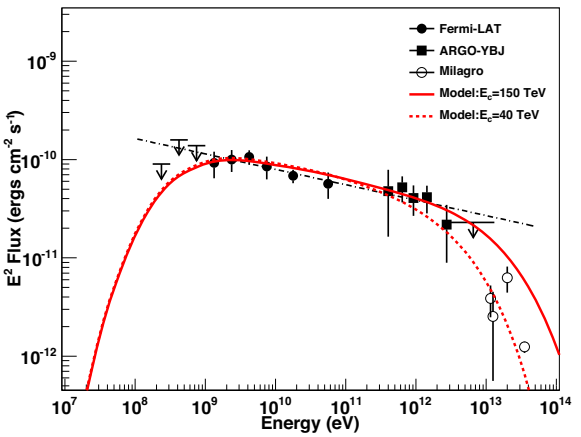

Figure 8: Spectrum of the Cygnus Cocoon as measured by different detectors. The arrows below 1 GeV indicate the upper limits set by Fermi/LAT, the Milagro data refer to MGRO J2031+41, at 12 TeV corrected for the extrapolation of TeV J2032+4130 [18]. The dot-dashed line shows the power law best fit to the combined Fermi/LAT and ARGO-YBJ data. The solid and dotted curves are predicted by a purely hadronic model with proton cutoff energy at 150 TeV and 40 TeV, respectively.

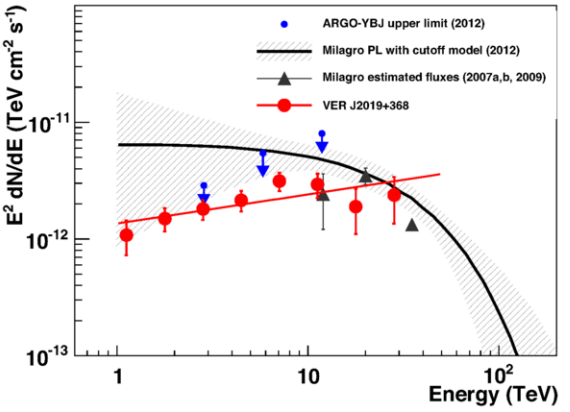

Figure 9: Observational results for MGRO J2019+37 from different experiments (figure taken from [23]). The Milagro power law with cutoff best fit, with its 1σ error band (shadowed area), is taken from [17].

power law with exponential cutoff, the maximum cutoff energy allowed by the ARGO-YBJ highest energy upper limit is E_c=150 TeV (solid line in Figure 8). Taking into account also the Milagro data, E_c would be around 40 TeV (dotted line).

Concerning MGRO J2019+37, which is the second brightest source after the Crab Nebula with Milagro data at ∼12 TeV, having an extension $\sigma_{ext} = 0.32^\circ \pm 0.12^\circ$ [22], the ARGO-YBJ map does not show any excess above 3 s.d., and flux upper limits were set at 90% confidence level (c.l.) [13]. The VERITAS observatory imaged MGRO J2019+37, resolving it into two different sources: the faint point-like VER J2016+371 and the bright extended (∼ 1°) VER J2019+368, which likely contributes to the bulk of the emission observed by Milagro and is spatially coincident with the pulsar PSR J2021+3651 and the star formation HII region Sh 2-104 [23]. The flux of VER J2019+368 is in agreement with the ARGO-YBJ upper limit. All these results are reported in Figure 9.

Considering also the ARGO-YBJ results for MGRO J1908+06 [24] and HESS J1841-055 [25], as for the Milagro air shower detector, the fluxes measured in extended sources are systematically larger than those measured with Cherenkov telescopes. The origin of this discrepancy, which is not present for point-like sources, is not clear. For ARGO-YBJ, the overall systematic error on the flux measurements has been estimated to be < 30% [26]. There could be some systematic effect related to the methods for background evaluation of the different experimental techniques [25].

Moreover, a contribution is expected from the diffuse gamma ray emission produced by the interaction of cosmic rays with matter in the Galactic plane, however, according to ARGO-YBJ measurements, it is different for each extended source but always less than 15% of the detected flux [27].

3. Diffuse gamma rays from the Galactic plane

The events collected by ARGO-YBJ have been analysed to determine the diffuse gamma ray emission in the Galactic plane at Galactic longitudes $25^\circ < l < 100^\circ$ and Galactic latitudes $|b| < 5^\circ$ [27]. This analysis was carried out in the energy range from ∼350 GeV to ∼2 TeV, connecting the region explored by Fermi/LAT with that investigated by Milagro. In particular, the analysis was focused on two selected regions of the Galactic plane, i.e., $40^\circ < l < 100^\circ$ and $65^\circ < l < 85^\circ$ (the Cygnus region), where Milagro observed an excess with respect to what predicted by current models.

In the Galaxy region $40^\circ < l < 100^\circ$, $|b| < 5^\circ$, after masking the discrete sources and subtracting the residual contribution, an excess with a statistical significance of 6.1 s.d. above the background is found. The spectral analysis provides the three fluxes shown in Figure 10, at median energies 350 GeV, 680 GeV and 1.47 TeV (with uncertainties of about 30%). The fit to the ARGO-YBJ data with a power law gives a spectral index -2.90 ± 0.31, and the corresponding flux at 1 TeV

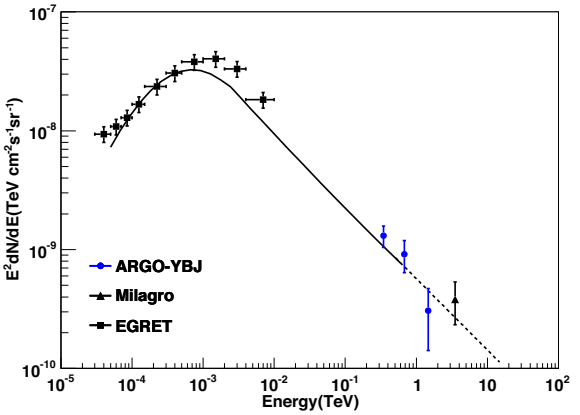

Figure 10: Energy spectrum of the diffuse gamma ray emission measured in the Galactic region $40° < l < 100°$, $|b| < 5°$. The line indicates the energy spectrum expected from the Fermi/LAT template (with spectral index -2.6, which also rules its short-dashed extension).

is compatible with the extrapolation of the Fermi/LAT template.

On the other hand, the first measurement of the diffuse TeV (integral) flux from the Galactic plane made by Milagro [28] revealed a "TeV excess" in the diffuse gamma ray spectrum with respect to expectations [29]. This Milagro measurement, converted into differential flux, is only 34% greater than the value expected from the extrapolation of the Fermi/LAT template, and within the experimental uncertainties (see triangle with error bars in Figure 10). Moreover, considering that the Milagro result does not take into account the contributions from the Cygnus Cocoon (not yet discovered at the time of the measurement) and from overlapping point and extended sources, the discrepancy with the Fermi/LAT predictions is almost cancelled out. Therefore, the full set of measurements with ground-based detectors is in agreement with direct observations by Fermi/LAT, and the evidence of any "TeV excess", requiring additional sources or particle production processes other than those producing Galactic cosmic rays, is ruled out.

In the Galactic region $65° < l < 85°$, $|b| < 5°$, after masking the discrete sources and the Cygnus Cocoon and subtracting the residual contribution, an excess of 4.1 s.d. is left. This direction points into our spiral arm at the remarkable Cygnus star-forming region, located at a distance of about 1.4 kpc, which is one of the sky regions best surveyed at all wavelengths from radio to gamma rays, including the measurements of Fermi/LAT and Milagro at GeV and TeV energies, respectively. Fermi/LAT data have been used to study the region $72° < l < 88°$, $|b| < 15°$, where the bright and extended Cygnus Cocoon was detected (see above). The spectral energy distribution of gamma ray emission is shown in Figure 11 (filled stars) together with the spectrum expected from the Fermi/LAT template (dot-dashed line). Milagro measured the diffuse gamma ray emission from the region $65° < l < 85°$, $|b| < 2°$ at a median energy of 15 TeV [30], obtaining the flux reported as a filled triangle in Figure 11. For comparison, the long-dashed line shows the expected energy spectrum for this region according to the Fermi/LAT template. The Milagro flux results about 75% higher than the Fermi template, suggesting the presence of an excess. The spectral analysis of ARGO-YBJ data provides the three fluxes shown in Figure 11 at median energies 440 GeV, 780 GeV and 1.73 TeV (with uncertainties of about 40%). The fit to ARGO-YBJ data with a power law gives a spectral index -2.65 ± 0.44, and the corresponding flux at 1 TeV is about 10% lower than the extrapolation of the Fermi/LAT template. These data do not show any excess at energies around 1 TeV which corresponds to the excess found by Milagro at a median energy of 15 TeV. Again, this discrepancy can be explained taking into account that the contribution of all the discrete gamma ray sources was not completely removed from the Milagro data. According to the ARGO-YBJ data, the 1 TeV flux associated to the Cygnus Cocoon is of the same order of the diffuse flux. Finally, the harder spectrum in the Cygnus region compared with that measured in the whole region $40° < l < 100°$, $|b| < 5°$ may suggest the presence of young cosmic rays accelerated by a nearby source.

4. Search for Gamma Ray Bursts in scaler mode

In scaler mode, the energy threshold for photons is about 1 GeV, lower than the highest energies detected by satellite experiments. Moreover, the modular structure of the ARGO-YBJ detector allowed the collection of data during the different mounting phases. Therefore a search for emission from Gamma Ray Bursts (GRBs) in coincidence with satellite detections started in November 2004, when the Swift satellite was launched [31]. Until February 2013 a sample of 206 GRBs was analysed, 24 of them with known redshift z. This is the largest sample of GRBs investigated with a ground-based detector at high energies. Figure 12 shows the distribution of the resulting significances for all the 206 GRBs (black solid line). No significant excess is found, the largest being 3.52σ for GRB 080727C, with a post-trial chance probability of 4.5×10^{-2}. Since long GRBs (duration T90 > 2 s) typically show a softer spectrum,

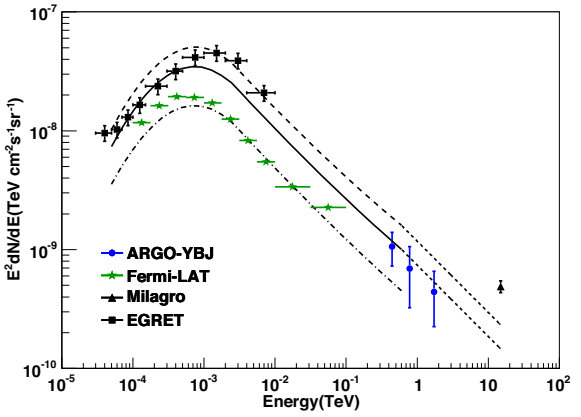

Figure 11: Energy spectrum of the diffuse gamma ray emission measured by ARGO-YBJ and EGRET in the Galactic region $65° < l < 85°$, $|b| < 5°$, by Milagro in the region $65° < l < 85°$, $|b| < 2°$ and by Fermi/LAT in $72° < l < 88°$, $|b| < 15°$. The different lines indicate the energy spectra expected from the Fermi/LAT template (with spectral index -2.6, which also rules their short-dashed extensions) in the different sky regions investigated by the detectors.

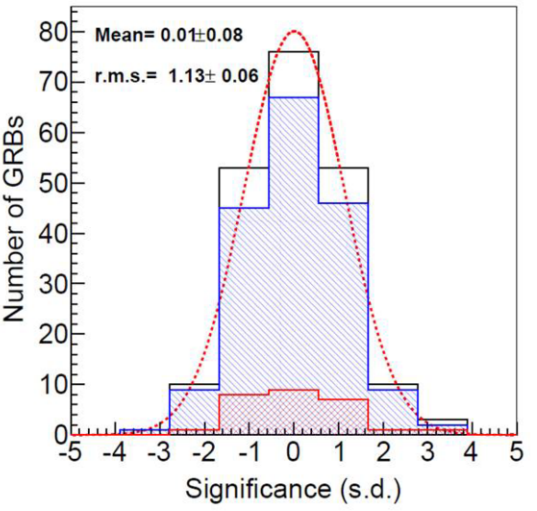

Figure 12: Distribution of the statistical significances of the 206 GRBs with respect to background fluctuations (black solid line) compared with a free Gaussian fit (dotted line, with mean value and r.m.s. given in the plot). The blue and red dashed distributions are for long and short GRBs, respectively.

the same distribution is shown in Figure 12 only for the 27 short GRBs (T90 $\leq$ 2 s, red dashed area). Also in this case, no significant excess is found, the most significant event being GRB 051114 with 3.37σ and a post-trial chance probability of 1.0×10^{-2}

Besides the coincidence analysis for each GRB, a stacked analysis was carried out in order to search for commom features of all GRBs in time or in phase. In the time analysis the counting rates for all the GRBs were added up in nine windows (Δt = 0.5, 1, 2, 5, 10, 20, 50, 100 and 200 s), starting at the trigger time, in order to investigate a possible common duration of the high energy emission. In the phase analysis only the 165 GRBs with duration T90 $\geq$ 5 s were added up, dividing their time length into ten bins each sampling 10% of T90 and scaling their duration to a common phase plot (in this case the lower limit on the GRB duration is due to the minimum interval, 0.5 s, for the scaler mode data acquisition and the number of bins considered). However, there is no evidence of any integral effect in both these analyses.

Since no significant signal was found in the data, for each GRB fluence upper limits in the 1-100 GeV energy range were determined at 99% c.l. assuming two different power law spectra: a) the index measured by satellite detectors in the keV-MeV energy range; b) the conservative differential index -2.5. For case a), when double power law spectral features have been identified, the higher spectral index (i.e., that above the peak in the keV-MeV region of the $E^2 \cdot dN/dE$ spectrum) has been used. For the set of 24 GRBs with known redshift the ranges of upper limits between the values corresponding to the two spectral assumptions are represented by rectangles in Figure 13, while a simple arrow is shown if the low energy spectrum is a cutoff power law, and thus only case b) is considered. These are the only upper limits set at GeV energies for these GRBs. For GRB090902B (which was the GRB in the ARGO-YBJ field of view with the highest photon energy detected) the fluence extrapolated from Fermi/LAT observations in the same energy range is also shown [32]. Only for this GRB the GeV spectral index measured by Fermi/LAT was used and the dashed area in Figure 13 was obtained with a maximum energy of the GRB spectrum ranging from 30 GeV (about the maximum energy measured by Fermi/LAT) to 100 GeV. More results and details about this search can be found in [33].

5. Summary

During the data taking with its full layout from November 2007 to February 2013, the ARGO-YBJ experiment detected six sources and five candidate sources in the sky survey of the northern hemisphere (declination band from -10° to 70°) with a sensitivity of 0.24 Crab unit. Continuous observation of the Crab Nebula

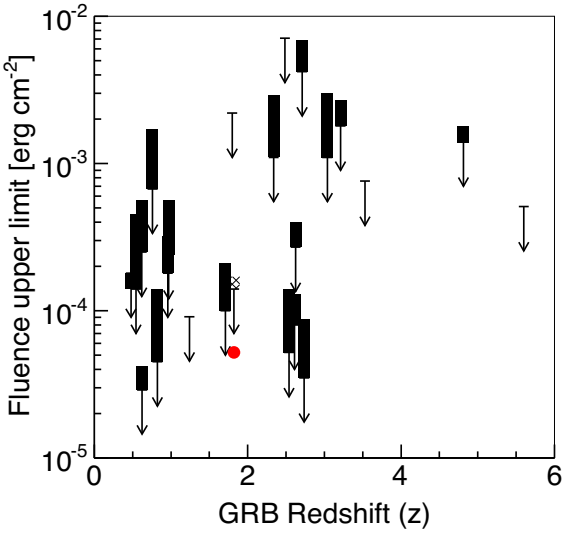

Figure 13: Fluence upper limits in the 1-100 GeV energy range for the 24 GRBs with known redshift, obtained with differential spectral indexes ranging from the value measured by satellites to -2.5 (only this latter case is considered for cutoff power law spectra). The dot shows the fluence extrapolated in the 1-100 GeV interval from the Fermi/LAT observations of GRB090902B (see text for its upper limit determination).

produced a spectrum in agreement with other experiments and a light curve compatible with a steady emission. Long-term monitoring of the blazars Mrk 421 and Mrk 501 allowed the investigation of their flaring states, also in correlation with other energy bands. Concerning extended sources, ARGO-YBJ identified the TeV counterpart of the Cygnus Cocoon and measured fluxes from MGRO J2031+41, MGRO J1908+06 and HESS J1841-055 in agreement with those determined by Milagro but systematically larger than those measured by Cherenkov telescopes, maybe because of the different methods for background evaluation in the two experimental techniques. Moreover, ARGO-YBJ detected diffuse gamma ray emission from the Galactic plane, without finding any excess at sub-TeV energies corresponding to that revealed by Milagro at higher energies. Using its scaler mode since November 2004 (when still in mounting phase), ARGO-YBJ searched for emission from GRBs in coincidence with satellite detections, and a sample of 206 GRBs (24 with known redshift) was analysed, being the largest sample of GRBs ever investigated with a ground-based detector at high energies. No significant signal was found in the data, and for each GRB fluence upper limits in the 1-100 GeV energy range were determined at 99% c.l. with two different assumptions on their power law spectra. For GRB090902B, the fluence extrapolated from Fermi/LAT observations in the same energy range is just a factor 2.7 lower than the ARGO-YBJ expected sensitivity.

References

[1] G. Aielli et al., *NIM A* **562** 92 (2006)
[2] G. Aielli et al., *Astropart. Phys.* **30** 85 (2008)
[3] B. Bartoli et al., *PRD* **84** 022003 (2011)
[4] B. Bartoli et al., *ApJ* **779** 27 (2013)
[5] A. U. Abeysekara et al., Submitted to *ApJ* (arXiv:1509.05401)
[6] T. P. Li & Y. Q. Ma, *ApJ* **272** 317 (1983)
[7] B. Bartoli et al., *ApJ* **798** 119 (2015)
[8] B. Bartoli et al., *ApJ* **758** 2 (2012)
[9] M. Amenomori et al., *ApJ* **532** 302 (2000)
[10] B. Bartoli et al., *ApJ* **734** 110 (2011)
[11] A. A. Abdo et al., *ApJ* **664** L91 (2007)
[12] P. L. Nolan et al., *ApJS* **199** 31 (2012)
[13] B. Bartoli et al., *ApJ* **745** L22 (2012)
[14] F. Aharonian et al., *A&A* **431** 197 (2005)
[15] J. Albert et al., *ApJ* **675** L25 (2008)
[16] A. A. Abdo et al., *ApJ* **700** L127 (2009)
[17] A. A. Abdo et al., *ApJ* **753** 159 (2012)
[18] M. Ackermann et al., *Science* **334** 1103 (2011)
[19] B. Bartoli et al., *ApJ* **790** 152 (2014)
[20] E. Aliu et al., *ApJ* **770** 93 (2013)
[21] L. O'C. Drury, F. Aharonian & H. J. Völk, *A&A* **287** 959 (1994)
[22] A. A. Abdo et al., *ApJ* **658** L33 (2007)
[23] E. Aliu et al., *ApJ* **788** 78 (2014)
[24] B. Bartoli et al., *ApJ* **760** 110 (2012)
[25] B. Bartoli et al., *ApJ* **767** 99 (2013)
[26] G. Aielli et al., *ApJ* **714** L208 (2010)
[27] B. Bartoli et al., *ApJ* **806** 20 (2015)
[28] R. Atkins et al., *PRL* **95** 251103 (2005)
[29] T. Prodanović, B. D. Fields & J. F. Beacom, *Astropart. Phys.* **27** 10 (2007)
[30] A. A. Abdo et al., *ApJ* **688** 1078 (2008)
[31] G. Aielli et al., *ApJ* **699** 1281 (2009)
[32] A. A. Abdo et al., *ApJ* **706** L138 (2009)
[33] B. Bartoli et al., *ApJ* **794** 82 (2014)